J. Fluid Mech. (2000), *vol.* 422, *pp.* 69–90. Printed in the United Kingdom

© 2000 Cambridge University Press

On Stokes flow in a semi-infinite wedge

By P. N. SHANKAR

Computational and Theoretical Fluid Dynamics Division, National Aerospace Laboratories, Bangalore 560 017, India
e-mail: pns@ctfd.cmmacs.ernet.in

(Received 29 September 1999 and in revised form 2 May 2000)

Consider Stokes flow in the semi-infinite wedge bounded by the sidewalls $\phi = \pm\alpha$ and the endwall $z = 0$. Viscous fluid fills the region $0 < r < \infty$, $0 < z < \infty$ bounded by these planes; the motion of the fluid is driven by boundary data given on the endwall $z = 0$. A consequence of the linearity of the problem is that one can treat the velocity field $\boldsymbol{q}(r, \phi, z)$ as the sum of a field $\boldsymbol{q}^a(r, \phi, z)$ antisymmetric in ϕ and one symmetric in it, $\boldsymbol{q}^s(r, \phi, z)$. It is shown in each of these cases that there exists a real vector eigenfunction sequence $\boldsymbol{v}_n(r, \phi, z)$ and a complex vector eigenfunction sequence $\boldsymbol{u}_n(r, \phi, z)$, each member of which satisfies the sidewall no-slip condition and has a z-behaviour of the form e^{-kz}. It is then shown that one can, for each case, write down a formal representation for the velocity field as an infinite integral over k of the sums of the real and complex eigenfunctions, each multiplied by unknown real and complex scalar functions $b_n(k)$ and $a_n(k)$, respectively, that have to be determined from the endwall boundary conditions. A method of doing this using Laguerre functions and least squares is developed. Flow fields deduced by this method for given boundary data show interesting vortical structures. Assuming that the set of eigenfunctions is complete and that the relevant series are convergent and that they converge to the boundary data, it is shown that, in general, there is an infinite sequence of corner eddies in the neighbourhood of the edge $r = 0$ in the antisymmetric case but not in the symmetric case. The same conclusion was reached earlier for the infinite wedge by Sano & Hasimoto (1980) and Moffatt & Mak (1999). A difficulty in the symmetric case when $2\alpha = \pi/2$, caused by the merger of two real eigenfunctions, has yet to be resolved.

1. Introduction

One of the most interesting and important general results in fluid mechanics is Moffatt's on the existence of corner eddies in plane, viscous flows. Moffatt (1964*a*, *b*) showed that, provided that the corner angle was not too large, the field in the neighbourhood of the corner would consist of an infinite number of eddies of decreasing size and strength. Although the result was deduced for Stokes flow, it was argued that it was likely to hold for all steady flows since the slow flow equations had to hold near the corner. The generalization of this result or the determination of its relevance to three-dimensional flows has proven to be difficult. Although Stokes' equations are linear and superposition holds, their vector structure in three dimensions is such that the usual linear methods do not apply in a straightforward manner.

It appears that the only studies in which a fully three-dimensional field involving a corner is investigated are Sano & Hasimoto (1978, 1980). Consider a corner of angle 2α bounded by two infinite planes. Since superposition is valid in Stokes flow it is convenient to consider flow fields symmetric and antisymmetric about the plane $\phi = 0$,

https://doi.org/10.1017/S0022112000001804 Published online by Cambridge University Press

where ϕ is the azimuthal angle. In the earlier paper Sano & Hasimoto determine the effect of the nearby walls on a settling sphere, while in the later paper they examine the nature of the corner eddies in this three-dimensional situation. Specifically, they consider the case of a Stokeslet driving the flow near the corner and conclude in the antisymmetric case that there is indeed an infinite sequence of eddies near the corner. For the symmetric case their results seem inconclusive. (However, it appears that in his thesis (Sano 1977), which Professor Sano was kind enough to send me, he was able to conclude that the result did not hold in the symmetric case.) A problem with the pioneering work of Sano & Hasimoto is that they use the Kontorovich–Lebedev transform which leads to complicated and difficult analysis. Thus the extension of the analysis to handle non-singular forcing is not obvious. V. Mak & H. K. Moffatt (1997, private communication), tackle the problem indirectly. They too consider the corner formed by two infinite planes but with forcing at the plane boundaries. First they show by an argument based on the equations averaged over the axial direction that, in general, there will be an infinite sequence of eddies in the antisymmetric case. Then, by developing an analytical solution for the flow between two parallel planes, they show that an infinite sequence of eddies does not exist for the symmetric case. In extending the result to the true corner case a limiting argument for the corner angle has to be used that appears not wholly satisfactory. Mak & Moffatt conclude their paper 'Results from the parallel plane problem suggest that perhaps for non-zero α there are no infinite eddy sequences in the symmetric flow'. The same problem is considered in Moffatt & Mak (1999); here the same conclusions are reached under the assumption that all fields are weakly varying in the z-direction.

A somewhat different approach was followed in Shankar (1998*b*), where an attempt was made to follow the path set out by Moffatt in two dimensions. First, complex eigenfunctions were found for both the antisymmetric and symmetric cases; the eigenvalues were exactly the same as those relevant to the plane case. Then the nature of the stagnation points and streamline patterns in the two cases was examined. It was then shown that Moffatt's arguments could be applied to these three-dimensional eigenfunctions to show the existence of corner eddies. The weakness in this work is that it does not consider the possibility of the existence of real eigenfunctions that can modify or destroy the structures of interest. In retrospect, this danger is inherent in any approach that does not consider a proper boundary value problem. It is this failure that is to be remedied here.

We shall pose and attempt to solve a precisely stated boundary value problem for Stokes flow near a semi-infinite wedge. The simplest situation that one can consider is shown in figure 1. The apex is bounded by three planes, $\phi = \pm\alpha$ and $z = 0$, and the fluid occupies the unbounded region $0 < r < \infty$, $-\alpha < \phi < \alpha$, $0 < z < \infty$. It should be noted that unlike the previous studies the axial extent is only semi-infinite. On the stationary sidewalls $\phi = \pm\alpha$ the boundary conditions are that the velocity $\boldsymbol{q} = (q_r, q_\phi, q_z)$ has to vanish. We will assume that sufficiently well behaved but arbitrary boundary data on the velocity are given on the endwall $z = 0$, i.e. $\boldsymbol{q} = \boldsymbol{q}_0 = (q_{0r}(r, \phi), q_{0\phi}(r, \phi), q_{0z}(r, \phi))$. And by requiring the velocity to decay in the far field we have fully specified the corner problem that we wish to solve. With the problem posed in this way a heuristic principle clearly points out the need for the existence of a real eigenvalue sequence in each case. We need to satisfy three scalar boundary conditions on the plane $z = 0$. Earlier experience with the planar case (Moffatt 1964*a*; Shankar 1993) and with other three-dimensional cases (Shankar 1997*a*, *b*, 1998*a*) indicates the need here for three real sequences or one complex one and one real one. Since we already have a suitable complex one, another real sequence has to be found for each case.

https://doi.org/10.1017/S0022112000001804 Published online by Cambridge University Press

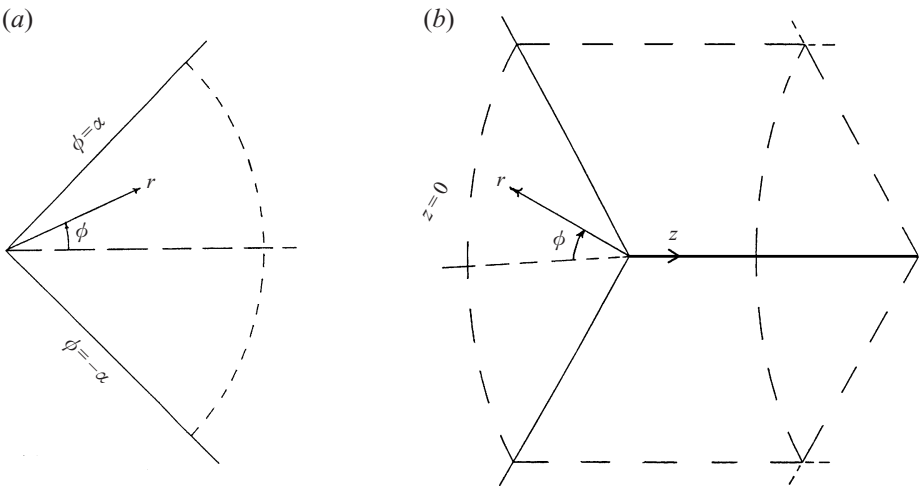


FIGURE 1. The three-dimensional corner and the cylindrical coordinate system used. Viscous fluid occupies the region $0 < r < \infty, 0 < z < \infty$ bounded by the sidewalls $\phi = \pm\alpha$ and the endwall $z = 0$. (*a*) Endview looking towards z, (*b*) perspective, looking towards the corner from the interior.

In § 2 we will recover the ingredients that were missing earlier while in § 3 the special tools required to handle the infinite interval will be developed.

2. Vector eigenfunctions and a formal expansion for the field

The method that we shall employ is the one using vector eigenfunctions (Shankar 1997*a*, *b*). Thus one must first find the relevant eigenfunctions. This task is simplified considerably by the use of a result that seems to have been known for some time (see for example Imai 1973) but which has been generalized more recently by Tran-Cong & Blake (1982). If $\boldsymbol{A}$ and B_0 are vector and scalar fields which satisfy Laplace's equation, then

$$\boldsymbol{q} = \nabla(\boldsymbol{r}\cdot\boldsymbol{A} + B_0) - 2\boldsymbol{A}, \tag{1a}$$

$$p = 2\mu(\nabla\cdot\boldsymbol{A}) \tag{1b}$$

are velocity and pressure fields that satisfy Stokes' equations. Thus it is sufficient to find suitable solutions to the scalar and vector Laplace equations appropriate to our geometry. The independence of the coefficients of Laplace's equation of ϕ and z suggests that we seek solutions of the form $f(r)\mathrm{e}^{\mathrm{i}\lambda\phi-kz}$, where λ and k are initially taken to be arbitrary scalars. However, since for the problem at hand we need the field to decay for $z \to \infty$, we shall take k to be positive. With these assumed forms one finds that $\boldsymbol{A}$ and B_0 are given by

$$A_z, B_0 \sim \mathrm{e}^{\mathrm{i}\lambda\phi-kz}J_\lambda(kr), \tag{2a}$$

$$(A_r, A_\phi) \sim \mathrm{e}^{\mathrm{i}\lambda\phi-kz}(J_{\lambda-1}(kr), \mathrm{i}J_{\lambda-1}(kr)), \tag{2b}$$

$$(A_r, A_\phi) \sim \mathrm{e}^{\mathrm{i}\lambda\phi-kz}(J_{\lambda+1}(kr), -\mathrm{i}J_{\lambda+1}(kr)), \tag{2c}$$

where A_r and A_ϕ cannot be chosen independently.

The relevant complex eigenfunctions were found and described in detail in Shankar (1998*b*). For the convenience of the reader they are briefly recapitulated. For the boundary conditions relevant here it is found that A_r and A_ϕ alone are sufficient to

https://doi.org/10.1017/S0022112000001804 Published online by Cambridge University Press

generate the complex eigenfunctions. It now proves convenient to solve for the fields antisymmetric and symmetric in ϕ separately. First, for the antisymmetric field choose

$$A_r = \{a \sin(\lambda+1)\phi + b \sin(\lambda-1)\phi\} J_\lambda(kr) \mathrm{e}^{-kz}, \tag{3a}$$

$$A_\phi = \{a \cos(\lambda+1)\phi + b \cos(\lambda-1)\phi\} J_\lambda(kr) \mathrm{e}^{-kz}, \tag{3b}$$

where some rearrangement of the indices has been done. With this vector field, formula (1) yields for the antisymmetric velocity field

$$u_r^a = \{a \sin(\lambda+1)\phi + b \sin(\lambda-1)\phi\}(rJ'_\lambda(kr) - J_\lambda(kr))\mathrm{e}^{-kz}, \tag{4a}$$

$$u_\phi^a = \{a(\lambda-1) \cos(\lambda+1)\phi + b(\lambda+1) \cos(\lambda-1)\phi\} J_\lambda(kr) \mathrm{e}^{-kz}, \tag{4b}$$

$$u_z^a = -kr\{a \sin(\lambda+1)\phi + b \sin(\lambda-1)\phi\} J_\lambda(kr) \mathrm{e}^{-kz}. \tag{4c}$$

On the other hand the corresponding symmetric velocity field is given by

$$u_r^s = \{c \cos(\lambda+1)\phi + d \cos(\lambda-1)\phi\}(rJ'_\lambda(kr) - J_\lambda(kr))\mathrm{e}^{-kz}, \tag{5a}$$

$$u_\phi^s = -\{c(\lambda-1) \sin(\lambda+1)\phi + d(\lambda+1) \sin(\lambda-1)\phi\} J_\lambda(kr) \mathrm{e}^{-kz}, \tag{5b}$$

$$u_z^s = -kr\{c \cos(\lambda+1)\phi + d \cos(\lambda-1)\phi\} J_\lambda(kr) \mathrm{e}^{-kz}. \tag{5c}$$

The primes in (4*a*) and (5*a*) indicate differentiation with respect to r. Now the no-slip boundary conditions on the sidewalls of the corner require that $u_r^a = u_\phi^a = u_z^a = 0$ on $\phi = \pm\alpha$ and similarly for the symmetric field (u_r^s, u_ϕ^s, u_z^s). It easily follows that for the $\boldsymbol{u}^a$ field, λ has to satisfy the equation

$$\sin 2\lambda\alpha = -\lambda \sin 2\alpha, \tag{6}$$

while the scalars a and b have to be related as follows:

$$b = -\frac{\sin(\lambda+1)\alpha}{\sin(\lambda-1)\alpha} a. \tag{7}$$

The corresponding results for the symmetric velocity field $\boldsymbol{u}^s$ are

$$\sin 2\lambda\alpha = \lambda \sin 2\alpha, \tag{8a}$$

$$d = -\frac{\cos(\lambda+1)\alpha}{\cos(\lambda-1)\alpha} c. \tag{8b}$$

It should be noted that the eigenvalue sequences are exactly the same as those that arose in the plane case. The three-dimensional velocity fields they generate are, naturally, quite different; some of their properties have been examined in Shankar (1998*b*).

Now we come to the real eigenfunctions $\boldsymbol{v}$, the constituents that have so far been missing. Before showing how the new sequences are generated we first point out that one real eigenfunction is already known to exist for the symmetric case. Inspection shows that $\lambda = 1$ is a solution of (8*a*) for all α and consequently the corresponding velocity field is a valid eigenfunction. The key to finding the other real eigenfunctions lies in the observation that this field has no azimuthal component of velocity, i.e. $u_\phi^s = 0$ if $\lambda = 1$ in (5*b*). Every streamline of this field lies throughout on the same azimuthal plane. This suggests that we look for fields of this type, i.e with no ϕ-component of velocity. For the antisymmetric fields, first rewrite (4) as follows:

$$v_r^a = [a^*(rJ'_{\lambda-1}(kr) - J_{\lambda-1}(kr)) + b^*(rJ'_{\lambda+1}(kr) - J_{\lambda+1}(kr)) + c^* J'_\lambda(kr)]\mathrm{e}^{-kz} \sin\lambda\phi, \tag{9a}$$

$$v_\phi^a = [a^*(\lambda-2)J_{\lambda-1}(kr) + b^*(\lambda+2)J_{\lambda+1}(kr) + c^*\lambda J_\lambda(kr)/r]\mathrm{e}^{-kz} \cos\lambda\phi, \tag{9b}$$

$$v_z^a = -k[a^* rJ_{\lambda-1}(kr) + b^* rJ_{\lambda+1}(kr) + c^* J_\lambda(kr)]\mathrm{e}^{-kz} \sin\lambda\phi. \tag{9c}$$

https://doi.org/10.1017/S0022112000001804 Published online by Cambridge University Press

Note that here we have added the c^*-dependent terms which come from the scalar potential B_0. Now, observing the form of v_ϕ^a and noting that $J_{\lambda-1}(kr) + J_{\lambda+1}(kr) = 2\lambda J_\lambda(kr)/r$ we choose $b^* = (\lambda-2)a^*/(\lambda+2)$. If we now set $c^* = -2(\lambda-2)a^*/k$ the azimuthal velocity component vanishes. The antisymmetric velocity field (9) then reduces to

$$v_r^a = a^*[(rJ'_{\lambda-1}(kr) - J_{\lambda-1}(kr)) + \frac{(\lambda-2)}{(\lambda+2)}(rJ'_{\lambda+1}(kr) - J_{\lambda+1}(kr)) - \frac{2(\lambda-2)}{k}J'_\lambda(kr)]\mathrm{e}^{-kz}\sin\lambda\phi, \tag{10a}$$

$$v_\phi^a = 0, \tag{10b}$$

$$v_z^a = -ka^*[rJ_{\lambda-1}(kr) + \frac{(\lambda-2)}{(\lambda+2)}rJ_{\lambda+1}(kr) - \frac{2(\lambda-2)}{k}J_\lambda(kr)]\mathrm{e}^{-kz}\sin\lambda\phi. \tag{10c}$$

Now, very nicely, the velocity will vanish on the sidewalls provided

$$\lambda = \mu_n^a = n\pi/\alpha, \quad n = 1, 2, 3, \ldots . \tag{11}$$

Thus the real eigenvalues and eigenfunctions that we sought for the antisymmetric case are given by (11) and (10) respectively. The corresponding eigenfunctions and eigenvalues for the symmetric case are found in a similar manner. The eigenfunctions are exactly as they are in (10), the only difference being that the ϕ-dependence is now $\cos\lambda\phi$ instead of $\sin\lambda\phi$. In this case the eigenvalues are given by

$$\lambda = \mu_n^s = (2n-1)\pi/(2\alpha), \quad n = 1, 2, 3 \ldots . \tag{12}$$

Now that we have the required eigenfunctions we are in a position to write down a formal expansion for the velocity field $\boldsymbol{q}(r, \phi, z)$. Since the boundary data can always be written as the sum of a part antisymmetric in ϕ and a part symmetric in it, we can deal with the two parts separately and then add them to get the total field. In order to reduce the notation we shall drop the superscripts a and s with the understanding that at any given time we are dealing with only one of them, which one being determined by the context. Let $\{\boldsymbol{v}_n(r, \phi, z; k),\ n = 1, 2, 3, \ldots\}$ be the real vector eigenfunctions correponding to the real sequence $\{\mu_n,\ n = 1, 2, 3, \ldots\}$ and $\{\boldsymbol{u}_n(r, \phi, z; k), n = 1, 2, 3, \ldots\}$ be the complex vector eigenfunctions corresponding to the complex sequence $\{\lambda_n,\ n = 1, 2, 3, \ldots\}$. Note that if we are dealing with symmetric fields $\boldsymbol{v}_1$ is the real eigenfunction corresponding to the solution $\lambda = 1$ in (8*a*). It should be noted that so far k is arbitrary. Guided by the potential problem for the corner shown in figure 1 with data given on $z = 0$, we now take k to be real (and positive for boundedness); further, in analogy with the Hankel transform solution for the potential problem we write

$$\boldsymbol{q}(r, \phi, z) = \int_0^\infty \sum_n \{b_n(k)\boldsymbol{v}_n(r, \phi, z; k) + \mathrm{Re}\{a_n(k)\boldsymbol{u}_n(r, \phi, z; k)\}\}\mathrm{d}k, \tag{13}$$

where $b_n(k)$ and $a_n(k)$ are respectively real and complex valued on the non-negative real line. The mathematically important questions regarding the completeness of these eigenfunctions, the convergence of the above series and whether the convergence near the endwall is to the boundary data are, in this genuinely three-dimensional vector field case, bound to be difficult to answer. Even in the two-dimensional case (see, for example, Gregory 1980 and Joseph, Sturges & Warner 1982), where one need only deal with the biharmonic equation for a scalar, results are strictly available

https://doi.org/10.1017/S0022112000001804 Published online by Cambridge University Press

only for canonical data (and the no-slip conditions are non-canonical) on the finite interval; it appears that no results are currently available in the higher dimensional case.

There is another apparent difficulty that should be pointed out here. We note on examining equations (4), (5) and (9), (10) that, whereas the azimuthal components of the velocity eigenfunctions decay as $r^{-1/2}$ in an oscillatory manner for $r \to \infty$, the radial and axial components actually grow as $r^{1/2}$ again in an oscillatory manner. One may fear that these components of the velocity field $\boldsymbol{q}$ may become unbounded as $r \to \infty$. But this difficulty can be avoided if the coefficients $a_n(k)$ and $b_n(k)$ in (13) are such that when the integration over k is performed all the components decay at infinity. And this, indeed, is what must happen. Although the computations that follow have their own limitations as will be seen, they do give some support to this conjecture. An analogy may be of help in this matter. Consider representing by a Fourier transform a real function on the real line which decays at infinity. Now although each individual Fourier mode is oscillatory and does not decay at infinity the integral over the wavenumber leads to the required decay.

Here, without proof we shall assume a favourable answer to these questions and proceed to the solution of the problem. Then the task reduces to: given $\boldsymbol{q} = \boldsymbol{q}_0(r, \phi)$ (where $\boldsymbol{q}_0(r, \phi)$ is known) on the plane $z = 0$ determine the *functions* $b_n(k)$ and $a_n(k)$. This task is much harder than the ones in Shankar (1997*a*, *b*, 1998*a*) where infinite sequences of scalars had to found rather than infinite sequences of functions.

3. Laguerre functions and least squares

It was shown in the last section that the formal solution to the flow in the wedge required the determination of the functions $b_n(k)$ and $a_n(k)$ on the positive real line. What is not feasible is to discretize the k-axis and try to determine the unknowns at the grid points. This is because the infinite integrals involve oscillatory integrands which need a fairly fine grid and long range, leading to a prohibitively large number of unknowns. What is proposed here is to represent $b_n(k)$ and $a_n(k)$ by known functions multiplied by unknown coefficients. This would reduce the problem once more to determining sequences of scalars and, if one chooses well, their number need not be prohibitively large. For this purpose we introduce the Laguerre functions $\mathscr{L}_m(k)$ which are defined as $\mathscr{L}_m(k) = \mathrm{e}^{-k/2} L_{m-1}(k)$, $m = 1, 2, 3, \ldots$, where $L_m(k)$, $m = 0, 1, 2, 3, \ldots$ are the Laguerre polynomials (Abramowitz & Stegun 1968). The first few Laguerre polynomials are $L_0(k) = 1$, $L_1(k) = 1 - k$ and $L_2(k) = 1 - 2k + k^2/2$. Some of the important properties of the Laguerre functions are (*a*) they form an orthonormal, complete set on the infinite interval, (*b*) $\mathscr{L}_m(0) = 1$ for all m, (*c*) they are oscillatory until their rapid decay for large k and (*d*) with increasing m the oscillatory range increases.

Now consider the integral equation (13) for the Stokes flow velocity field $\boldsymbol{q}(r, \phi, z)$ in the wedge given that $\boldsymbol{q} = \boldsymbol{q}_0(r, \phi)$ on the endwall $z = 0$. As suggested we expand $b_n(k)$ and $a_n(k)$ in terms of the Laguerre functions as follows:

$$b_n(k) = \sum_m \beta_{nm} \mathscr{L}_m(k), \quad n = 1, 2, 3 \ldots, \tag{14a}$$

$$a_n(k) = \sum_m \alpha_{nm} \mathscr{L}_m(k), \quad n = 1, 2, 3 \ldots, \tag{14b}$$

where now the real scalars β_{nm} and the complex scalars α_{nm} have to be determined.

https://doi.org/10.1017/S0022112000001804 Published online by Cambridge University Press

Substituting (14) into (13) we have

$$\boldsymbol{q}(r,\phi,z) = \sum_n \sum_m \left[\beta_{nm} \left\{ \int_0^\infty \mathscr{L}_m(k) \boldsymbol{v}_n(r,\phi,z;k)\,\mathrm{d}k \right\} + \mathrm{Re}\left(\alpha_{nm} \left\{ \int_0^\infty \mathscr{L}_m(k) \boldsymbol{u}_n(r,\phi,z;k) \right\} \mathrm{d}k \right) \right] \tag{15}$$

In order to determine the β_{nm} and α_{nm}, we now set $z = 0$ in the above expression and require that $\boldsymbol{q}$ take the boundary data $\boldsymbol{q}_0(r,\phi)$. In this form the use of the least-squares procedure used in Shankar (1997*a*, *b*, 1998*a*) becomes feasible although here the minimization will be on the whole plane rather than on a finite segment. Since the least total error squared procedure has been discussed in the earlier papers we only outline it here. By symmetry we need only deal with half the corner $0 \leqslant \phi < \alpha$. Let this azimuthal range be divided into J equal segments. On each of the J radial lines choose I radial points, not necessarily equidistant. The error minimization will be done on these $L = I \times J$ points. Now choose the first N real and complex eigenfunctions and the first M Laguerre functions. Assuming the integrals over k in (15) are done numerically using a constant step size Δk choose its value and the number of steps K to give an adequate range. Thus in (15) the sums are over N and M respectively and the upper limit of the integral is $K\Delta k$. Define the error squared at any one of the L test points to be $|\boldsymbol{q} - \boldsymbol{q}_0|^2$ evaluated there with $\boldsymbol{q}$ given by (15). Now the least-squares procedure consists in choosing the $N^* = 3N \times M$ real unknowns in such a way that the total error squared over the L test points is a minimum. This leads to a system of N^* linear algebraic equations which can be solved by standard routines. One additional small but important point: the condition $b_n(0) = a_n(0) = 0\ \forall n$ needs to be enforced at the expense of $3N$ of the highest-order error minimization equations. One naturally expects the results to improve as N and M are increased.

Before trying this procedure on the complicated Stokes flow problem it was tested on the far simpler problem of determining the potential in the wedge of figure 1 given data on the endwall $z = 0$. The advantage in this case is that the results of the present method can be carefully compared with the exact solution given by the use of a Hankel transform. The results, outlined in the Appendix, were very encouraging.

In order to compactly specify the boundary data in what follows let us define one radial and three azimuthal functions as follows:

$$\mathscr{R}(r;r_0,r_1) = \begin{cases} 0, & r < r_0 \\ \dfrac{1}{2}\left\{1 - \cos\dfrac{2\pi(r-r_0)}{(r_1-r_0)}\right\}, & r_0 \leqslant r \leqslant r_1 \\ 0, & r > r_1, \end{cases} \tag{16a}$$

$$\Phi_1(\phi) = \cos\frac{\pi\phi}{2\alpha}, \quad \Phi_2(\phi) = 1 - \left(\frac{\phi}{\alpha}\right)^2, \quad \Phi_3(\phi) = \sin\frac{\pi\phi}{\alpha}. \tag{16b}$$

Note that $\mathscr{R}(r)$ vanishes outside the segment (r_0, r_1) and is continuous and smooth inside it, taking a maximum value of 1. $\Phi_1(\phi)$ and $\Phi_2(\phi)$ are even functions of ϕ while $\Phi_3(\phi)$ is odd; all of them vanish on $\phi = \pm\alpha$. We shall need to distribute the minimization points non-uniformly in the radial direction. Let $\Delta = 1/I$; then define the set of I radial points by $\mathscr{P}(I) = \{r_1, r_2, \ldots r_I\}$ where $r_l = \tan(l\pi\Delta/2)$. This set of points is distributed non-uniformly in r with an adequate number of points where we shall drive the flow and still have enough, spaced increasingly far apart, for large r.

It might not be out of place to indicate the steps that were taken to ensure that

https://doi.org/10.1017/S0022112000001804 Published online by Cambridge University Press

the calculations were reasonably accurate. The Bessel functions $J_\nu(x)$ do need some care in their evaluation since the orders are large and the arguments are unbounded. The integral representations (9.1.21) and (9.1.22) of Abramowitz & Stegun (1968) were used for Bessel functions of real and complex order respectively; for the infinite integral in the latter formula an asymptotic expansion was used for moderately large values of the argument. In both cases when the argument was large the asymptotic formula for large argument (7.13.1(3)) of Erdeli (1953) was used. Many computations were done to determine the minimum step size required to accurately evalute the oscillatory integrals and to determine when the asymptotic formula could be used. For example, while the default step size on the finite integral on $[0, \pi]$ in the complex case was $\pi/10\,000$, for $124 < \mathrm{Re}\,\nu < 164$ and $x < 2000$ the step size was one half of the default; for $x > 2000$ the asymptotic formula was used. The aim, in this manner, was to compute the eigenfunctions to an accuracy of 10 significant figures or better and we believe this was achieved using double-precision arithmetic. The solution of (13) requires the solution of a large linear system of equations. Here the checks included confirming that the residuals were small when the solution was back substituted into the equations, checking whether increasing the precision (quadruple precision) made any difference to the solution and, most important, whether the boundary data were reproduced to reasonable accuracy.

Although many tests were done and checks were carried out, for the results that follow the relevant parameters are $N = 10$, $M = 40$, $I = 2M$, $J = 3N$, $\Delta k = 0.1$, $K = 1500$. It must be emphasized that there is nothing special or magical about this choice of parameters. Roughly, M must be large enough for accuracy along individual radial lines, N must be large enough to ensure accuracy along the azimuth. The number of minimization points must be much larger than the number of unknowns; we have chosen this factor to be 2. Other reasonable choices will lead to slightly different values for the coefficients but will not affect the fields significantly.

How well the boundary conditions can be satisfied is shown in figure 2 for an antisymmetric field driven by purely azimuthal forcing when $2\alpha = \pi/2$. In this case we have chosen

$$\boldsymbol{q}_0(r, \phi) = (0, \mathscr{R}(r; 1, 2)\Phi_1(\phi), 0) \tag{17}$$

so that only q_ϕ is non-zero on the boundary; it takes its maximum value of 1 on $\phi = 0$ and smoothly decays to the sidewalls. Each frame of figure 2 shows the computed values of the three components of velocity and $q_{0\phi}$ (solid line) on a different radial line; again the equally spaced points do not belong to $\mathscr{P}(I)$. Here the agreement is very good. Although not shown, the peaks are captured very well and the situation is as good on other radial lines. Naturally, it may be possible to choose other $\boldsymbol{q}_0$ for which the agreement is not as good as this. We find that the symmetric fields do cause more problems, giving less accuracy for a given set of parameters. But generally our experience is that as N and M are increased the boundary data can be better approximated. We therefore conjecture with much confidence that the representation (13) is a valid one and conclude that the present technique is reasonably satisfactory. In the next section we present the results of some computations in order to display some interesting features of these wedge flow fields.

4. Flow fields near the apex of the wedge

We first consider the simpler antisymmetric flows assuming that the wedge angle $2\alpha = \pi/2$. Table 1 lists the first ten complex eigenvalues λ_n^a while the real eigenvalues

https://doi.org/10.1017/S0022112000001804 Published online by Cambridge University Press

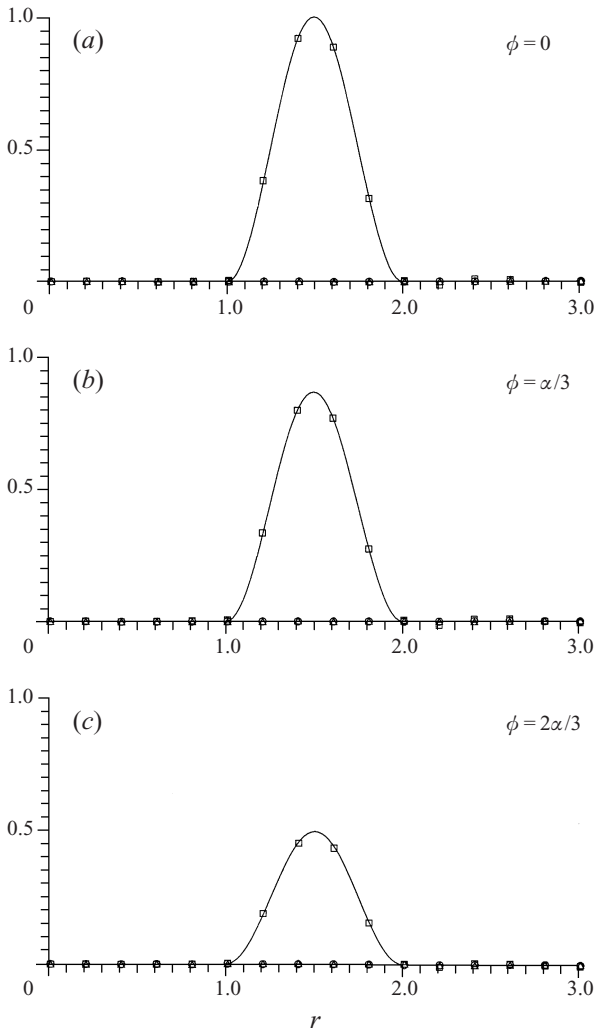


FIGURE 2. Effectiveness of the use of Laguerre functions and the least-squares procedure in the solution of the viscous flow problem in the wedge. The computed velocity components on $z = 0$ compared with the input data; antisymmetric case, azimuthal forcing. $\bigcirc, q_r$; $\square, q_\phi$; $\triangle, q_z$.

μ_n^a are given by (11); the latter are all integers in this case. A property useful in the calculation of the complex eigenvalues is that $\mathrm{Re}\,(\lambda_n - \lambda_{n-1}) \to 4$ as $n \to \infty$, i.e. for large n their spacing is almost the same as the constant spacing between the real eigenvalues. We first consider the case of purely azimuthal forcing on the boundary described by (17). In table 2 are listed the first ten Laguerre expansion coefficients for $b_1(k), a_1(k), b_2(k)$ and $a_2(k)$. Although only 4 decimal places have been given in both the tables all calculations have been carried out using at least double-precision arithmetic; for the larger systems of equations where the relevant matrices tend to be ill-conditioned quadruple-precision arithmetic has been used.

Figure 3 shows two views of eight streamlines in this antisymmetric field. One first notes that near the endwall all the streamlines lie primarily in the azimuthal direction, just as one would expect. Where and how they close, however, depends upon their location: those lying near the middle of the region of forcing close in the z-direction,

https://doi.org/10.1017/S0022112000001804 Published online by Cambridge University Press

Antisymmetric field	Symmetric fields	
$2\alpha = \pi/2$	$2\alpha = \pi/3$	$2\alpha = \pi/2$
2.73959+1.11902 i	7.18196+2.45567 i	4.80825+1.46393 i
6.84514+1.68163 i	13.28602+3.01714 i	8.86883+1.84238 i
10.88555+1.97020 i	19.33511+3.36646 i	12.89809+2.07642 i
14.90789+2.16733 i	25.36444+3.62134 i	16.91579+2.24683 i
18.92231+2.31746 i	31.38419+3.82225 i	20.92780+2.38103 i
22.93249+2.43880 i	37.39850+3.98813 i	24.93655+2.49177 i
26.94010+2.54066 i	43.40940+4.12942 i	28.94324+2.58606 i
30.94603+2.62843 i	49.41801+4.25247 i	32.94854+2.66816 i
34.95080+2.70555 i	55.42500+4.36147 i	36.95285+2.74087 i
38.95472+2.77433 i	61.43079+4.45929 i	40.95644+2.80612 i

TABLE 1. The first ten complex eigenvalues relevant to viscous flow near a corner of wedge angle 2α for the antisymmetric and symmetric cases.

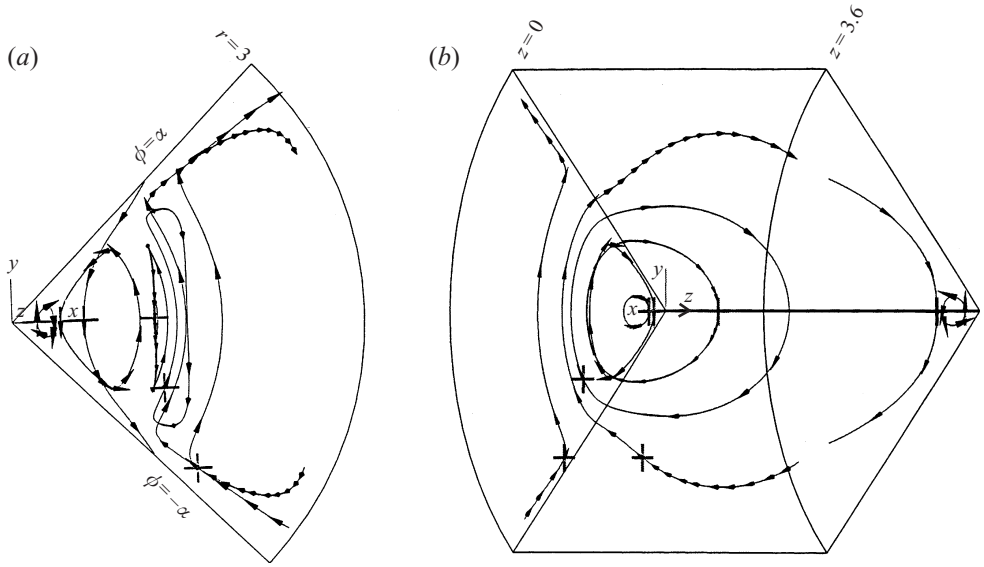


FIGURE 3. Two views of the same eight streamlines in the antisymmetric field with purely azimuthal forcing. The two views are the same as in figure 1 with $2\alpha = \pi/2, 0 < r < 3, 0 < z < 3.6$. Note that (*a*) is a projection of the three-dimensional streamlines on the endplane.

those lying inwards close near the edge $r = 0$, while those lying outwards tend to close at larger radial distances. In the figure only five streamlines close in the region shown. But it should be noted that by symmetry all streamlines which cut the plane $\phi = 0$ twice have to be closed. In this flow field it appears that all streamlines are closed. The most interesting feature of figure 3 is that it shows the existence of a corner eddy near the edge $r = 0$: to the right of figure 3(*b*) can be seen one streamline in the primary flow and a small, closed neighbouring streamline in the corner region. The corner eddy near the edge is examined more closely in figure 4(*a*). Streamlines generated by tracers released at two z-stations are shown. What is most evident is the role of three-dimensionality; while for small z the axial motion is dominant distorting the streamlines, for large z the eddy streamlines are almost planar. These features are

https://doi.org/10.1017/S0022112000001804 Published online by Cambridge University Press

https://doi.org/10.1017/S0022112000001804 Published online by Cambridge University Press

m	β_{1m}	α_{1m}	β_{2m}	α_{2m}
1	0.1245	$-0.2782 - 0.1759$ i	-0.8437×10^{-1}	$0.2199 \times 10^{-1} + 0.3471 \times 10^{-1}$ i
2	-0.2704×10^{-1}	$0.1152 + 0.3402$ i	-0.3915×10^{-1}	$0.6837 \times 10^{-2} - 0.1391 \times 10^{-1}$ i
3	-0.9925×10^{-1}	$0.3489 + 0.1828$ i	-0.5058×10^{-1}	$-0.1566 \times 10^{-2} + 0.4162 \times 10^{-1}$ i
4	-0.2699×10^{-1}	$0.2508 - 0.1921$ i	-0.6572×10^{-1}	$0.2072 \times 10^{-1} + 0.3463 \times 10^{-1}$ i
5	0.8587×10^{-1}	$-0.6872 \times 10^{-1} - 0.4215$ i	-0.3610×10^{-1}	$0.2927 \times 10^{-1} - 0.3311 \times 10^{-2}$ i
6	0.1464	$-0.3846 - 0.3511$ i	-0.4756×10^{-3}	$0.1376 \times 10^{-1} - 0.2783 \times 10^{-1}$ i
7	0.1217	$-0.4977 - 0.3946$ i	0.1101×10^{-1}	$-0.1136 \times 10^{-1} - 0.2391 \times 10^{-1}$ i
8	0.3631×10^{-1}	$-0.3386 + 0.3170$ i	0.3008×10^{-3}	$-0.2584 \times 10^{-1} - 0.8339 \times 10^{-3}$ i
9	-0.5553×10^{-1}	$0.6959 \times 10^{-2} + 0.5117$ i	-0.1316×10^{-1}	$-0.1968 \times 10^{-1} + 0.2135 \times 10^{-1}$ i
10	-0.1055	$-0.3559 + 0.4405$ i	-0.1433×10^{-1}	$0.1283 \times 10^{-2} + 0.2653 \times 10^{-1}$ i

TABLE 2. The first ten real and complex coefficients in the expansion in terms of Laguerre functions of $b_1(k), a_1(k), b_2(k)$ and $a_2(k)$.

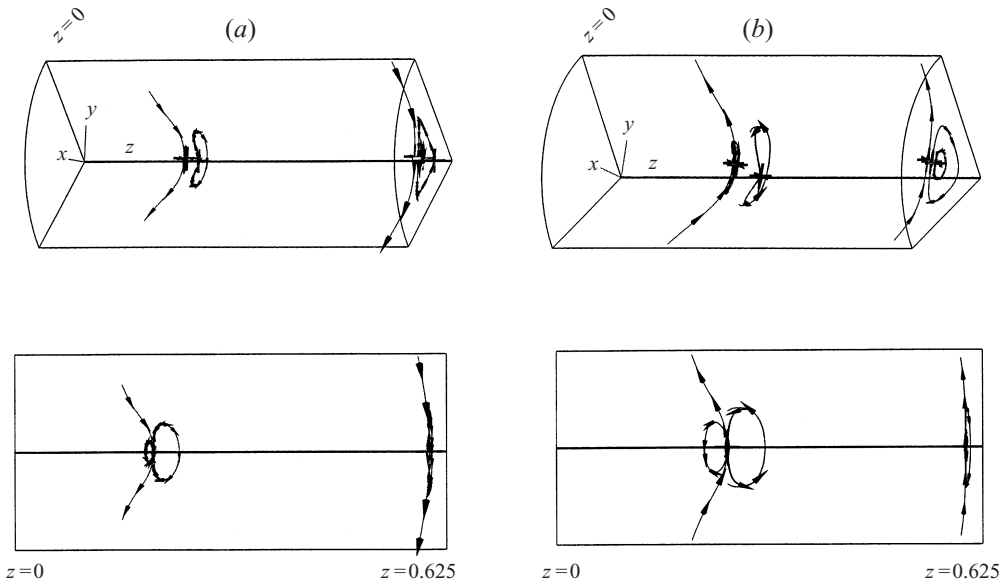


FIGURE 4. Corner eddies in the neighbourhood of the edge $r = 0$ in antisymmetric flows. Upper views are perspectives looking towards the corner while the lower ones are sideviews looking directly at the edge. $2\alpha = \pi/2, 0 < r < 0.2, 0 < z < 0.625$. (*a*) Azimuthal forcing, (*b*) radial forcing.

very reminiscent of what was found in Shankar (1998*b*). It is clear that the field here is dominated by the first complex eigenfunction.

We can also consider antisymmetric fields generated by purely radial forcing. Assume that the boundary data are given by

$$\boldsymbol{q}_0(r, \phi) = (\mathscr{R}(r; 1, 2)\Phi_3(\phi), 0, 0). \tag{18}$$

Now the only non-zero component is the radial one which vanishes on the plane of symmetry and on the sidewalls and takes its maximum value of 1 on $\phi = \alpha/2$. Some streamlines in the same region as that shown in figure 3 are shown in figure 5. This is a more interesting field. The endview, figure 5(*a*), clearly shows that near the strip where forcing is taking place on the endwall the streamlines tend to move radially outward, as we might expect. Again all streamlines which cut $\phi = 0$ twice are closed. But in this field there exist sidewall vortices from which streamlines emanate which cut the symmetry plane only once: these are not closed and go from one stagnation region to the other. Some streamlines near a sidewall vortex core are shown in figure 6. The stagnation points appear to be foci. One is naturally interested in whether corner eddies exist near the edge $r = 0$. That they indeed do is shown in figure 4(*b*). Although the forcing is so different in the two cases the corner eddies look very similar. While the forcing affects the scales, the general features are determined entirely by the principal complex eigenfunction. We shall return to this later.

The fact that the integral equation (13) has had to be solved numerically in the present work leads to certain limitations that should be pointed out. In figure 7(*a*) are plotted the velocity components (q_r, q_ϕ, q_z) along a single radial line at an azimuthal angle of $\pi/6$ and a distance $z = 0.5$ from the endwall. The situation is very similar along other radial lines and at other distances from the endwall. In the neighbourhood of the forcing region the field is well behaved with good simulation of the forcing field; further on, the field decays slowly as is normal with Stokes flow. Here, however,

https://doi.org/10.1017/S0022112000001804 Published online by Cambridge University Press

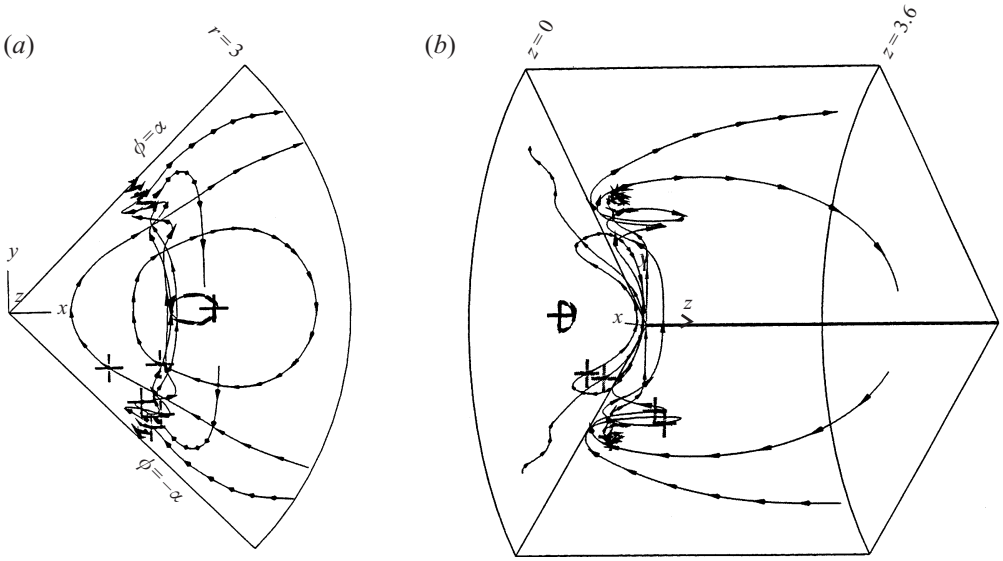


FIGURE 5. Streamlines in antisymmetric flow with radial forcing. The view and the region are the same as in figure 3.

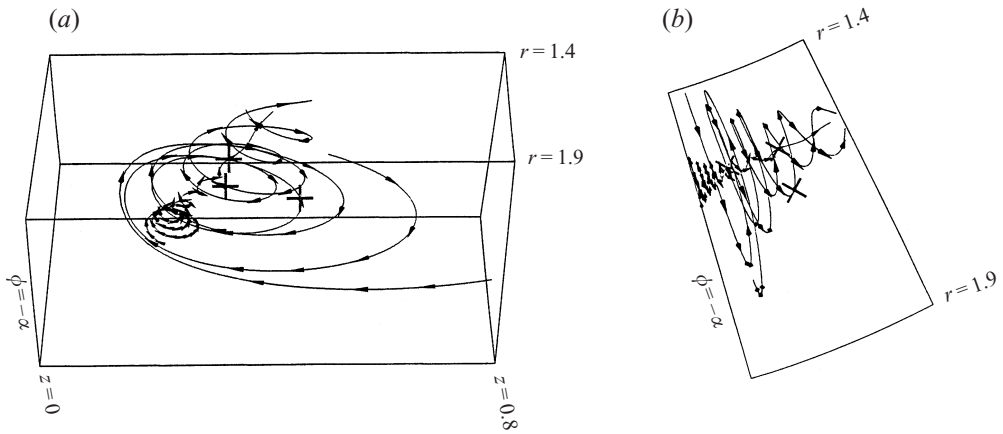


FIGURE 6. Detail of one of the sidewall vortices seen in figure 5. The streamline in the core emerges from a source-like focus on the endwall $\phi = -\alpha$ and flows into a sink-like focus on $\phi = \alpha$.

a little beyond $r = 25$ the velocity components begin to display oscillatory behaviour with comparatively large amplitudes for the radial and axial components. The reason for this unphysical behaviour is that in numerically solving (13) we have been able only approximately to achieve the cancellations that are necessary to ensure full decay for $r \to \infty$. As a consequence one should expect the radial and axial components to grow as $r^{1/2}$ in an oscillatory manner as $r \to \infty$.

It must be emphasized that this is not an indication of the failure of (13) but of the natural limitation of any numerical procedure used to invert integral transforms. This is clearly shown in the other two frames of the figure. Figure 7(*b*) shows the distribution along a radial line of the potential $\Psi(r, \phi, z)$ discussed in the Appendix. If Ψ had been computed using the exact Hankel inversion formula (A 1*b*) we would

https://doi.org/10.1017/S0022112000001804 Published online by Cambridge University Press

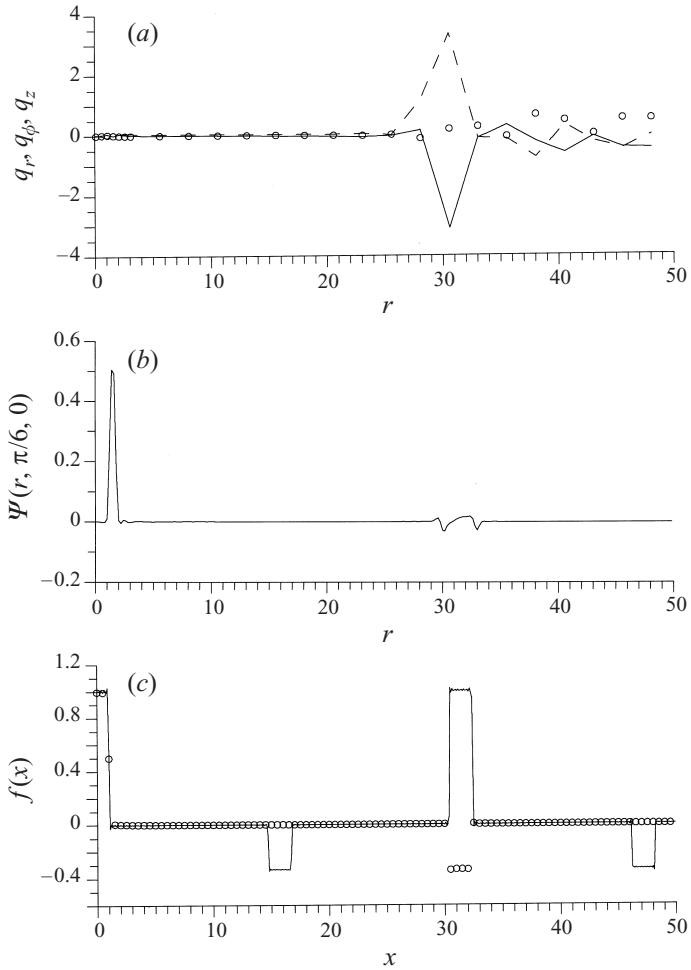


FIGURE 7. Far-field oscillations resulting from the numerical inversion of transforms. (*a*) Antisymmetric wedge flow with radial forcing, $\phi = \pi/6, z = 0.5$: ——, q_r; ○, q_ϕ; – – –, q_z. (*b*) The potential $\Psi(r, \phi, z)$ discussed in the Appendix. (*c*) Numerical Fourier inversion of the half-top-hat profile: ——, $\Delta k = 0.2$; ○, $\Delta k = 0.1$.

only see the bump at the left; but when the numerical procedure is used with $\Delta k = 0.1$ we get in addition the oscillation around $r = 30$ because of imperfect cancellations. These oscillations decay slowly as $r^{-1/2}$ as $r \to \infty$. One should not be misled by the small amplitude of the oscillations; the velocity is given by the gradient of Ψ and its amplitudes will be large. The oscillations seen in figure 7(*c*) are even more instructive. Consider the real function $f(x)$ on the real line given by $f(x) = 1, 0 \leqslant x < 1; f(1) = 0.5; f(x) = 0, x > 1$. Its Fourier cosine transform is given by $F(k) = \sin(k)/k$. Naturally the inversion using contour integration leads to the exact result, which is the bump seen to the left in figure 7(*c*). Now if we do the inversion numerically over $0 \leqslant k \leqslant 100$ using Simpson's rule with $\Delta k = 0.2$ we find three extra oscillations around $r = 15, 30$ and 45 respectively; note that the amplitude of the middle one is equal to that of the input. These oscillations repeat indefinitely because of the imperfect cancellation of the non-decaying Fourier modes. Decreasing Δk only postpones the appearance of the oscillations.

https://doi.org/10.1017/S0022112000001804 Published online by Cambridge University Press

In summary, numerical inversion will lead to oscillations as $r \to \infty$ and these do not indicate a failure of the basic theory but a limitation of the numerical procedure. The appearance of the oscillations can be postponed by improving the procedure, for example by decreasing Δk, but can never be completely eliminated. The only cure is an exact inversion formula but for the vector fields considered here in equation (13) such a formula does not exist at present. So for now we will have to use numerical procedures with the limitation that the results will hold only for small and moderate values of r. The present calculations appear to be reasonably accurate up to a radial distance of about 20.

We now come to the more complex and difficult case of symmetric fields. Here we shall assume the corner angle 2α to be $\pi/3$. The relevant complex eigenvalues are given in table 1 while the real eigenvalues except the first are given by (12); we take the first real one to be the single real solution, $\lambda = 1$, to (8*a*). The observation that $\mathrm{Re}(\lambda_n - \lambda_{n-1}) \to 6$, the common spacing of the real eigenvalues (beyond $n = 1$!), is helpful in computing them. Let us first consider the field when the forcing at the boundary is purely azimuthal:

$$\boldsymbol{q}_0(r, \phi) = (0, \mathscr{R}(r; 1, 2)\Phi_3(\phi), 0). \tag{19}$$

Now $q_{0\phi}$, the only non-vanishing component, vanishes on the symmetry plane and the sidewalls while taking its maximum value on $\phi = \alpha/2$. Some of the streamlines in this complex flow are shown in figure 8. Frames (*a*) and (*b*) show a sideview and an endview of the same four stream lines, two of which are among those that constitute the strong vortex just above the strip over which forcing is taking place. Both views clearly show the primarily azimuthal response to the forcing in the neighbourhood of the endwall. What is interesting about the vortex is that the streamlines that form the core seem to emanate from a structure in the fluid that is very reminiscent of a focus. This can be seen more clearly in frame (*c*): it appears as though the central streamline in the core will connect two stagnation points on either side, the 'foci'. This has not been investigated carefully. Of the other two streamlines one is of interest because it moves close to the edge $r = 0$, where a corner eddy might be. Note that all it does is make a loop in the region before sweeping outwards. There does not seem to be a corner eddy near the edge.

Lastly we consider the case of radial forcing in the symmetric case. Let the boundary conditions be given by

$$\boldsymbol{q}_0(r, \phi) = (\mathscr{R}(r; 1, 2)\Phi_1(\phi), 0, 0). \tag{20}$$

Now q_{0r}, the only non-zero component, takes its maximum on the symmetry plane and decays smoothly to zero on the sidewalls. The corresponding streamlines are shown in figure 9. Again we have a very strong vortex adjacent to the sector over which boundary forcing is taking place but now its axis is along the azimuthal direction rather than the radial direction. In frames (*a*) and (*b*) it is part of a single open streamline that is shown in the vortex. Frame (*c*), with two streamlines belonging to the vortex one of which is in the core, clearly shows that the stagnation point on the symmetry plane is a source-like focus. Three streamlines in the corner region along the edge $r = 0$ are shown in frame (*d*). All of them make single loops in this region before exiting; there is no evidence of a corner eddy. One should note that in both figure 8 and figure 9 only one half of the corner ($0 < \phi < \alpha$) is shown; the field in the other half can be inferred by symmetry. Also to be noted is that whereas most streamlines (and all those cutting $\phi = 0$ twice) are closed in antisymmetric fields, most if not all streamlines are open in symmetric fields.

https://doi.org/10.1017/S0022112000001804 Published online by Cambridge University Press

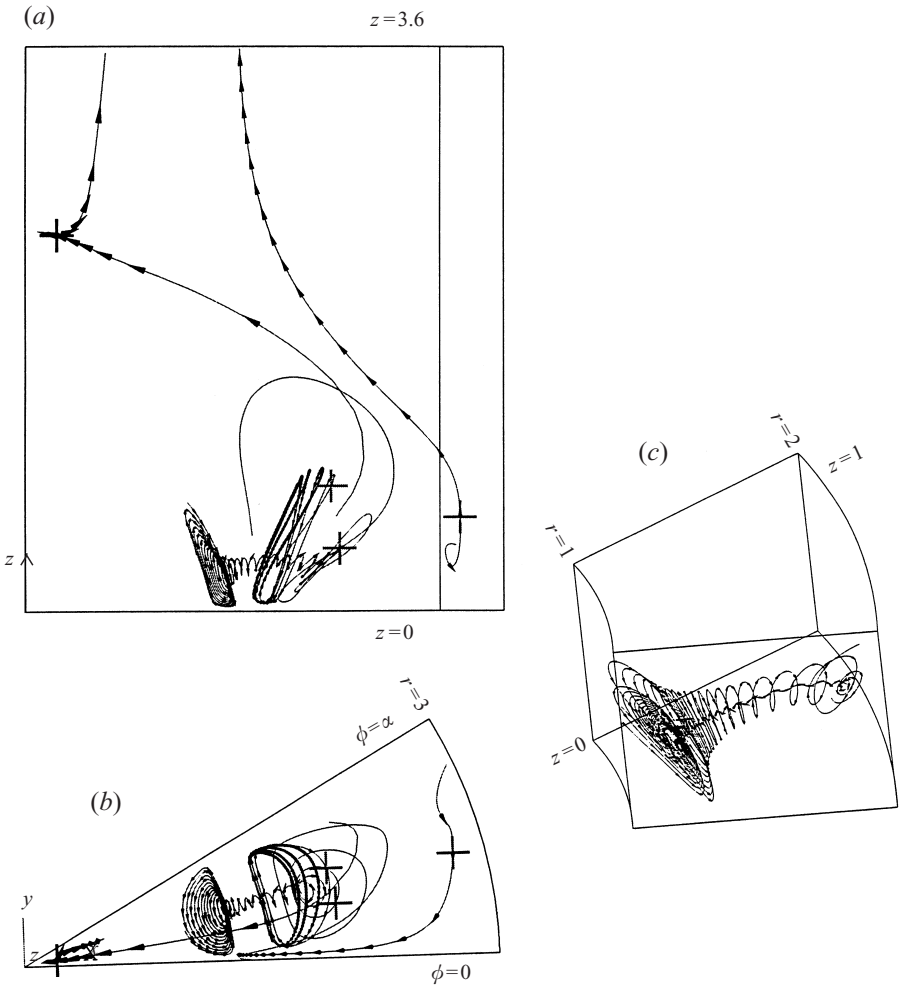


FIGURE 8. Streamlines in symmetric flow with azimuthal forcing; $2\alpha = \pi/3$. Note that only one half of the corner field is shown; the other half can be inferred from symmetry. (*a*) An end view, (*b*) the view looking towards $z, 0 < r < 3, 0 < z < 3.6$. A detail of the radial vortex is shown in (*c*).

5. Discussion

We now discuss certain shortcomings of the theory and calculational procedure that have been suggested above. As in many other cases of non-standard, non-self-adjoint problems the question of the completeness of the set of vector eigenfunctions is an open one. This is true even for planar Stokes flow problems such as those considered in Shankar (1993). While the question of completeness is important mathematically, all the computational evidence so far points to the soundness of the theory. On the other hand the present theory is incomplete, although for a very small subset of the parameter space! There is a difficulty in the symmetric case when the corner angle is $\pi/2$. Consider the real eigenvalues given by (12). As $2\alpha \to \pi/2$, $\mu_1^s \to 2$ and actually takes that value when $2\alpha = \pi/2$. Although it is not immediately obvious from (10) the corresponding eigenfunction turns out to be identical to the real eigenfunction associated with the single real eigenvalue of (8*a*), the dominant one. The merger of the two real eigenfunctions immediately signals trouble – in all probability another

https://doi.org/10.1017/S0022112000001804 Published online by Cambridge University Press

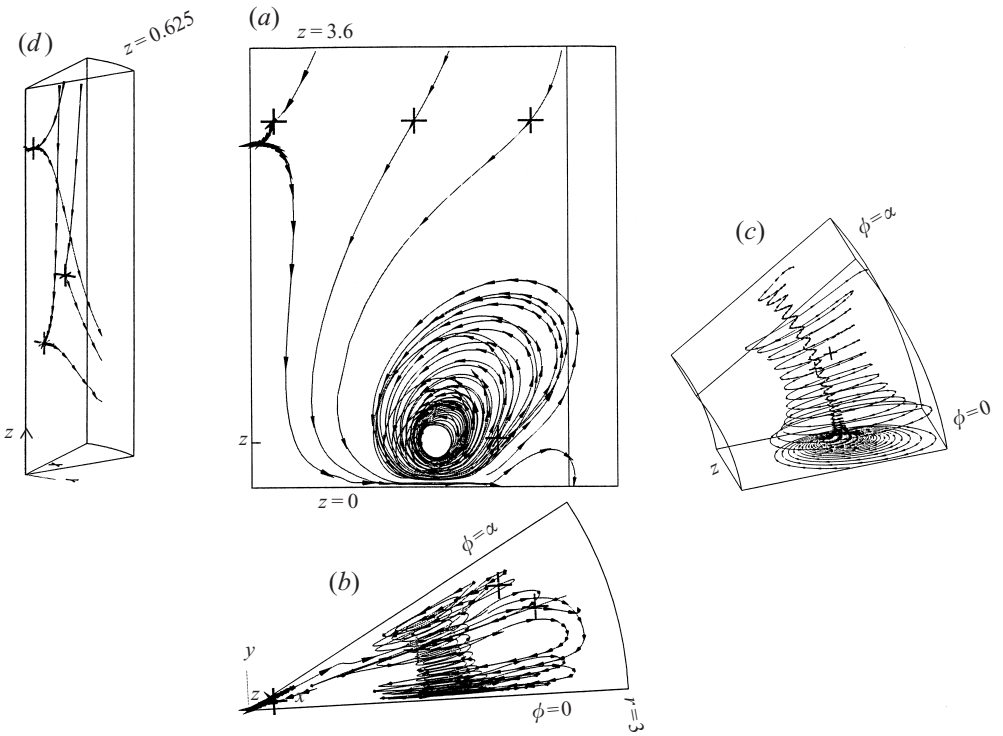


FIGURE 9. Streamlines in symmetric flow with radial forcing; $2\alpha = \pi/3$. Note that only one half of the corner field is shown. (a, b) As in figure 8. (c) A detail of the azimuthal vortex. (d) Streamlines in the corner region near $r = 0$.

eigenfunction needs to be found for this case. It is interesting that Sano & Hasimoto (1980), in the last paragraph of their paper dealing with a related corner problem, mention a similar difficulty for $2\alpha = \pi/2$. We are able to construct a harmonic function similar in form to the one given in their paper.† However, it has not been possible so far to find a way to combine this with other suitable forms to satisfy the boundary conditions. We have yet to resolve this difficulty and so it remains an open issue.

There is an important feature of the calculational procedure that this difficulty highlights. If one tries to calculate the symmetric field for $2\alpha = \pi/2$ by just dropping one of the twin eigenfunctions one finds that one cannot enforce the boundary conditions satisfactorily. This is illustrated in figure 10 where the results of applying the same procedure with the same parameters for $2\alpha = \pi/3$ and $2\alpha = \pi/2$ are compared. In the former case the boundary conditions are satisfied reasonably well, but in the latter very poorly. Although not shown, even more telling is the fact that increasing the number of eigenfunctions does not help at all. This is most reassuring; one should not be able to get by by adding higher-order terms if a lower-order term is missing. This shows how robust and reliable the method of least squares is.

Another feature that is evident from figure 10 is that even for other angles the symmetric case presents more computational problems. If we compare, ignoring the difference in corner angle, figure 10(a) with figure 2(a) we observe that for the same

† Professor Sano has pointed out in correspondence that there is a misprint in their paper. The expression for the new eigenfunction should read $r^2\left[\ln r \cos 2\theta - \theta \sin 2\theta + \pi/4\right]$. This expression vanishes on the sidewalls.

https://doi.org/10.1017/S0022112000001804 Published online by Cambridge University Press

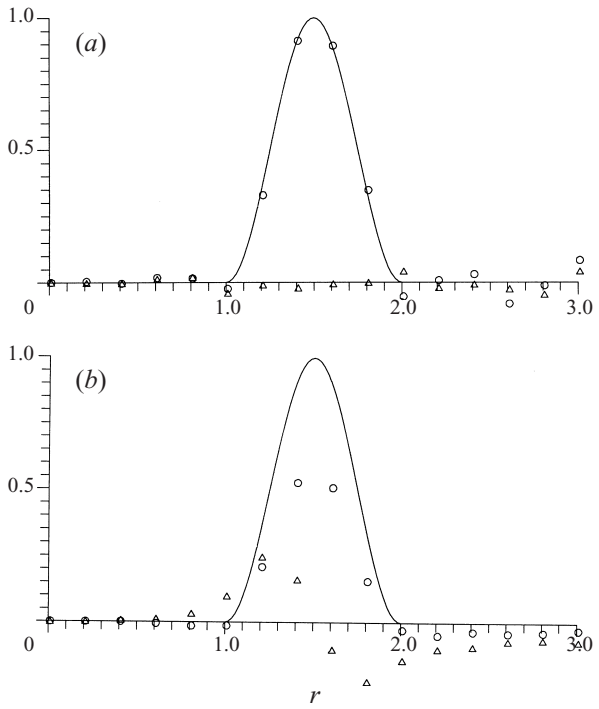


FIGURE 10. Failure of the expansion for a symmetric field when $2\alpha = \pi/2$. Symbols represent computed endwall velocity components while the solid lines are the given input data. (*a*) $2\alpha = \pi/3$, (*b*) $2\alpha = \pi/2$. $\bigcirc, q_r$; $\triangle, q_z$.

parameters the errors are greater in the symmetric case than in the antisymmetric case. This appears to be generally true. Finally it should be pointed out that there are difficulties with the least-squares procedure as the number of equations increases: the matrix associated with the system of equations for the unknowns becomes increasingly ill-conditioned. Increased precision does help but there are limitations.

Now we come to the issue of the corner eddies along the edge $r = 0$. We follow in this context a modified version of the arguments given in Moffatt (1964*a*) for the two-dimensional case. The field for $r \to 0$ will be dominated by the eigenfunction corresponding to the dominant eigenvalue, i.e. the one with the smallest real part. Here we need to take into account both the real sequence and the complex sequence of eigenvalues. First, for the antisymmetric case consider the azimuthal component of velocity, q_ϕ, on the plane of symmetry $\phi = 0$. By (13) it can be written as sums of integrals $q_\phi(r, 0, z) = \sum I_r + \mathrm{Re} \sum I_c$, corresponding to the real and complex eigenvalues. Each integral is of the form $I = \int_0^\infty a(k) J_\lambda(kr) \exp(-kz)\, \mathrm{d}k$. If we now substitute the series representation for the Bessel function and interchange the order of summation and integration we find that I is given by

$$I = \sum_l \frac{(-1)^l r^{\lambda+2l}}{2^{\lambda+2l} l! \Gamma(\lambda + l + 1)} \int_0^\infty a(k) k^{\lambda+2l} \exp(-kz)\, \mathrm{d}k. \tag{21}$$

It is now clear that for $r \to 0$ I will be dominated by the integral corresponding to the smallest λ in the real case and by the one with smallest real part in the complex case. In the antisymmetric case it is found that $\mathrm{Re}(\lambda_1^a)$ is always smaller than μ_1^a, e.g. for $2\alpha = \pi/2$ we have ~ 2.74 compared to 4. Thus the first complex eigenfunction $\boldsymbol{u}_1$

https://doi.org/10.1017/S0022112000001804 Published online by Cambridge University Press

will dominate and we can write

$$q^a_\phi|_{\phi=0} \sim \mathrm{Re}[(A^* + \mathrm{i}B^*)(r)^{\lambda_1}] \tag{22}$$

for the azimuthal component of velocity. Writing $\lambda_1 = \lambda_{1r} + \mathrm{i}\lambda_{1i}$ we find from (22)

$$q^a_\phi|_{\phi=0} \sim \gamma(r)^{p_1} \sin[p_2 \ln(r) + \epsilon]. \tag{23}$$

As $r \to 0$, q^a_ϕ keeps changing sign, indicating that the field consists of an infinite sequence of eddies. The computational evidence in § 4 shows the existence of the first eddy in the sequence for both the cases considered.

The situation is quite different when we consider symmetric fields. Here, we always have the one real eigenvalue ($\lambda = 1$) in (5*b*) which is always the smallest real eigenvalue for $2\alpha \leqslant \pi/2$. Now in this case the component that we need to consider is the radial component q_r. Further, it is easy to show that $v^s_{r1} \sim rJ_2(kr) \sim r^3$ as $r \to 0$. On the other hand, λ_1 keeps decreasing as α increases but, as table 1 shows, even at $\alpha = \pi/2$, $\mathrm{Re}\{\lambda_1\} \sim 4.8$ and so the real eigenvalue always dominates. Hence there will not be an infinite sequence of eddies. This result contrasts strikingly with the result in the plane (Moffatt 1964*a*) that infinite sequences of eddies exist in both cases. The present results are in conformity with what had been found earlier by Sano & Hasimoto (1980), V. Mak & H. K. Moffatt (1997, private communication) and Moffatt & Mak (1999) for the case of three-dimensional corner eddies near the edge of an infinitely long wedge, i.e where $-\infty < z < \infty$ and there is no endwall.

6. Conclusion

We have developed in this paper a method, based on a vector eigenfunction expansion, to describe the Stokes flow field in a semi-infinite wedge driven by prescribed data on the endwall. The main contributions of this paper are (*a*) the generation of the new real sequences of vector eigenfunctions (10) for the antisymmetric and symmetric cases, (*b*) the writing down of the representation (13) for the velocity field $\boldsymbol{q}(r, \phi, z)$ and (*c*) devising a computational procedure based on Laguerre functions and least squares to render the formalism tractable. Evidence has been presented in § 4 to show that the method can be used to examine these complex flow fields in some detail; the results show interesting vortical structures that cannot easily be surmised without such calculations. Finally, we have shown, subject only to mathematical questions of completeness and convergence, that in general an infinite sequence of corner eddies will exist in the neighbourhood of the edge $r = 0$ in the antisymmetric case but not in the symmetric case. This conclusion is in agreement with those of earlier authors for a different geometry.

I would like to thank Professor H. K. Moffatt for insisting, while refereeing a previous paper, that the real eigenfunctions had to play an important role. My thanks also go to Professors O. Sano, V. V. Meleshko and H. A. Stone for suggestions that led to improvements in this paper and for comments that helped to clarify related issues.

Appendix

It is instructive, before attempting the Stokes flow problem for the wedge as formulated in § 2, to examine a simpler problem for which we know the solution. Let $\Psi(r, \phi, z)$ be harmonic in the region shown in figure 1, and let us assume that Ψ takes

https://doi.org/10.1017/S0022112000001804 Published online by Cambridge University Press

well-behaved boundary data $\Psi_0(r,\phi)$ on $z=0$, which is symmetric in ϕ and vanishes on the sidewalls of the wedge. It is a simple matter to represent the boundary data in the form of a Fourier series $\Psi_0(r,\phi)=\sum_{n=1}^{\infty}\cos\nu_n\phi f_n(r)$, where the eigenvalues $\nu_n=(2n-1)\pi/(2\alpha), n=1,2,3\ldots$, enforce the sidewall conditions. Then the solution for Ψ most easily follows from an application of the Hankel transform

$$\Psi(r,\phi,z)=\int_0^{\infty}\sum_n^{\infty}kc_n(k)J_{\nu_n}(kr)\mathrm{e}^{-kz}\cos\nu_n\phi\,\mathrm{d}k, \tag{A 1a}$$

$$c_n(k)=\int_0^{\infty}rf_n(r)J_{\nu_n}(kr)\mathrm{d}r. \tag{A 1b}$$

Note that for every n the function $c_n(k)$, the Hankel transform of the data, is known explicitly from the formula (A 1b).

The question now is: what might one do if one had the representation (A 1a) but was unaware of the inversion formula (A 1b). This would then be analogous to our situation with regard to formula (13). The idea now is to represent the unknown $c_n(k)$ in terms of the Laguerre functions $\mathscr{L}_m(k)$ defined in § 3 and so we write

$$c_n(k)=\sum_m\gamma_{nm}\mathscr{L}_m(k),\ n=1,2,3\ldots, \tag{A 2}$$

where the unknowns now are the real scalars γ_{nm}. If the representation (A 2) is now substituted into (A 1a) and the orders of the sums and the integral are interchanged one gets

$$\Psi(r,\phi,z)=\sum_n\sum_m\cos\nu_n\phi\left\{\int_0^{\infty}k\mathscr{L}_m(k)J_{\nu_n}(kr)\mathrm{e}^{-kz}\mathrm{d}k\right\}\gamma_{nm}. \tag{A 3}$$

In order to determine the γ_{nm}, we now set $z=0$ in the above expression and require that Ψ take the boundary data $\Psi_0(r,\phi)$. In this form the use of the least-squares procedure becomes feasible. By symmetry we need only deal with half the corner $0\leqslant\phi<\alpha$. As described in §3 we distribute $L=I\times J$ points in the plane, choose the first N eigenfunctions and the first M Laguerre functions and perform the integrals using K points spaced Δk apart. Now the minimization need only be done for the scalar Ψ over the L points to determine the $N^*=N\times M$ scalars γ_{nm}. One additional small but important point: the condition $c_n(0)=0\ \forall n$ needs to be enforced at the expense of N of the highest-order error minimization equations.

In order to demonstrate how well the procedure works we consider the actual results of calculations for given boundary data. For the example considered here the boundary data are taken to be given by

$$\Psi_0(r,\phi)=\mathscr{R}(r;1,2)\Phi_2(\phi), \tag{A 4}$$

where $\mathscr{R}$ and Φ_2 are defined in (16). Thus Ψ_0 vanishes outside the segment $(1,2)$ on all radial lines, is symmetric in ϕ, takes its maximum value on $\phi=0$ and satisfies the sidewall conditions. The technique described above was applied with $N=5, M=40, I=2M$ and $J=3N$ with the error minimization being applied on the set $\mathscr{P}(I)$ of radial points on the J equal-angularly spaced radial lines. For the integrals over k, Δk was 0.1 and K was taken to be 1000. The results of the computation are shown in figure 11. In figure 11(a) the computed field on the endplane is compared with the given data (A 4) at equidistant points on three radial lines. Note that the agreement is good even at these points which do not belong to $\mathscr{P}(I)$; the situation

https://doi.org/10.1017/S0022112000001804 Published online by Cambridge University Press

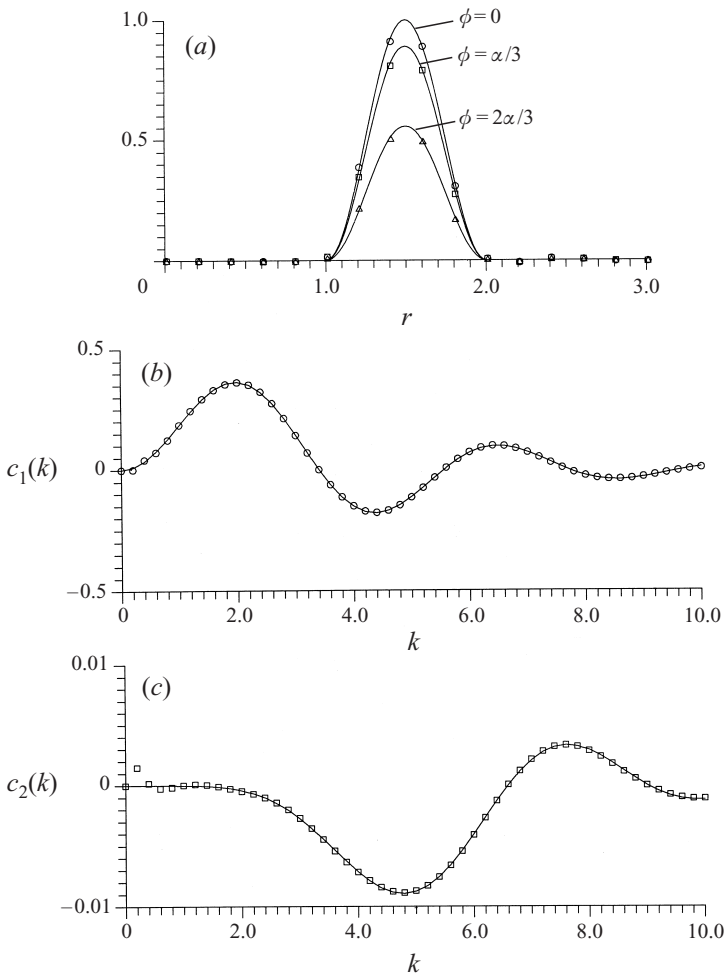


FIGURE 11. Effectiveness of the use of Laguerre functions and the least-squares procedure in solving $\nabla^2\Psi = 0$ in the wedge, given $\Psi(r, \phi, 0)$. Symbols represent computed values while solid lines represent input data or exact results. (*a*) $\Psi(r, \phi, 0)$ and $\Psi_0(r, \phi)$ on three radial lines, (*b*) $c_1(k)$ and (*c*) $c_2(k)$.

is just as good on other radial lines. A more difficult test is how well the coefficients $c_n(k)$ are calculated by this procedure. While figure 11(*b*) shows that $c_1(k)$ agrees very well with the exact result (A 1*b*) over the whole range of k shown, figure 11(*c*) indicates that there are discrepancies for small k; it is generally found that the errors occur for small k and are reduced by increasing N and M. It may be noted that these very reasonable results have been achieved using just five eigenfunctions. This gives reason to be optimistic in applying this technique for the Stokes flow problem.

REFERENCES

ABRAMOWITZ, M. & STEGUN, I. A. (Eds.) 1968 *Handbook of Mathematical Functions*. Dover.

ERDELYI, A. (Ed.) 1953 *Higher Transcendental Functions*, vol. II. McGraw-Hill.

GREGORY, R. D. 1980 The semi-infinite strip $x \geqslant 0$, $-1 \leqslant y \leqslant 1$; completeness of the Papkovich-Fadle eigenfunctions when $\phi_{xx}(0, y), \phi_{yy}(0, y)$ are prescribed. *J. Elast.* **10**, 57.

https://doi.org/10.1017/S0022112000001804 Published online by Cambridge University Press

Imai, I. 1973 *Ryutai Rikigaku* (*Fluid Mechanics*), vol. 1. Syokabo, Tokyo (in Japanese).

Joseph, D. D., Sturges, L. D. & Warner, W. H. 1982 Convergence of biorthogonal series of biharmonic eigenfunctions by the method of Titchmarsh. *Arch. Rat. Mech. Anal.* **78**, 223.

Moffatt, H. K. 1964*a* Viscous and resistive eddies near a sharp corner. *J. Fluid Mech.* **18**, 1.

Moffatt, H. K. 1964*b* Viscous eddies near a sharp corner. *Arch. Mech. Stosow.* **2**, 365.

Moffatt, H. K. & Mak, V. 1999 Corner singularities in three-dimensional Stokes flow. In *IUTAM Symp. on Non-Linear Singularities in Deformation and Flow*, p. 21. Kluwer.

Sano, O. 1977 Slow motion of a small sphere in a viscous fluid bounded by two plane walls. PhD Thesis, University of Tokyo.

Sano, O. & Hasimoto, H. 1978 The effect of two plane walls on the motion of a small sphere in a viscous fluid. *J. Fluid Mech.* **87**, 673.

Sano, O. & Hasimoto, H. 1980 Three-dimensional Moffatt-type eddies due to a Stokeslet in a corner. *J. Phys. Soc. Japan* **48**, 1763.

Shankar, P. N. 1993 The eddy structure in Stokes flow in a cavity. *J. Fluid Mech.* **250**, 371.

Shankar, P. N. 1997*a* Three-dimensional eddy structure in a cylindrical container. *J. Fluid Mech.* **342**, 97.

Shankar, P. N. 1997*b* A three-dimensional flow suggested by meniscus roll coating. N. A. L. document PD CF 9707. Also presented at *the 8th Asian Congress of Fluid Mechanics, Shenzhen, China, Dec. 6–10, 1999.*

Shankar, P. N. 1998*a* Three-dimensional Stokes flow in a cylindrical container. *Phys. Fluids* **10**, 540.

Shankar, P. N. 1998*b* On a class of three-dimensional corner eddies. *Pramāna – J. Phys.* **51**, 489.

Tran-Cong, T. & Blake, J. R. 1982 General solution of the Stokes' flow equations. *J. Math. Anal. Appl.* **90**, 72.

https://doi.org/10.1017/S0022112000001804 Published online by Cambridge University Press